Competing Exchange Interactions and Ground-State Variability: Linear Homo- and Heterotrinuclear Manganese(III, IV) Complexes with Tris(dimethylglyoximato)metalate(II) Tetraanions as Bridging Ligands

Frank Birkelbach,[†] Ulrich Flörke,[‡] Hans-Jürgen Haupt,[‡] Christian Butzlaff,[§] Alfred X. Trautwein,[§] Karl Wieghardt,[†] and Phalguni Chaudhuri*,[†]

Max-Planck Institut für Strahlenchemie, P.O. Box 101365, D-45413 Mülheim an der Ruhr, Germany, Anorganische und Analytische Chemie, Universität-Gesamthochschule Paderborn, D-33098 Paderborn, Germany, and Institut für Physik, Medizinische Universität zu Lübeck, D-23538 Lübeck, Germany

Received March 27, 1997

Two series of linear homo- and heterotrinuclear complexes, $Mn^{III}M^{II}Mn^{III}$ and $Mn^{IV}M^{II}Mn^{IV}$, where M^{II} represents Mn^{II} (**1** and **5**), Ni^{II} (**2** and **6**), Cu^{II} (**3** and **7**), or Zn^{II} (**4** and **8**), containing three dimethylglyoximato dianions (dmg^{2-}) as bridging ligands and 1,4,7-trimethyl-1,4,7-triazacyclononane (L) as the capping ligand for the terminal Mn^{III} or Mn^{IV} ions, have been synthesized. Compounds **1**−**8** have been characterized on the basis of elemental analyses, IR, UV−vis, and EPR spectroscopy, and variable-temperature (2−295 K) magnetic susceptibility measurements. The trinuclear complexes are quasi-isostructural with the terminal manganese ions in a distorted octahedral environment, $Mn^{III/IV}N_3O_3$, and the divalent metal ions M are six-coordinate with the $M^{II}N_6$ chromophore. The molecular structures of the compounds $[LMn^{III}\{(\mu\text{-dmg})_3Mn^{II}\}Mn^{III}L](ClO_4)_2$ (**1**) and $[LMn^{III}\{(\mu\text{-dmg})_3Cu^{II}\}Mn^{III}L](ClO_4)_2$ (**3**) have been established by X-ray diffraction. **1** crystallizes in the monoclinic system, space group $C2/c$, with cell constants $a = 32.472(6)$ Å, $b = 9.058(2)$ Å, $c = 16.729(3)$ Å, $\beta = 107.60(3)°$, $V = 4690.2(16)$ Å^3, and $Z = 4$. The crystal data for **3** are as follows: monoclinic, space group $C2/c$, $a = 32.686(5)$ Å, $b = 8.870(1)$ Å, $c = 16.867(2)$ Å, $\beta = 108.65(1)$, $V = 4633(1)$ Å^3, and Z = 4. Analyses of the susceptibility data indicate the presence of weak to moderate exchange interactions, both ferro- and antiferromagnetic, between the paramagnetic centers. It has been conclusively demonstrated that there are indeed two different coupling constants, $J = J_{12} = J_{23}$ and J_{13}, operative in these linear trinuclear complexes. J_{13} represents the exchange interaction between two terminal paramagnetic centers separated by a distance of ∼7 Å. The effect of J_{13} on the energy-splitting pattern has been demonstrated by the variability of the ground states. A qualitative rationale has been provided for the difference in magnetic behaviors. The cyclic voltammograms of complexes **1**−**8** reveal two reversible and two quasireversible one-electron redox processes. The central divalent metal ion in these complexes is redox-inactive.

Introduction

Exchange-coupled clusters of transition metal ions are relevant to many different scientific areas, ranging from chemistry to solid-state physics and to biology. There is a clear interest from the bioinorganic community, because of the emergence of an increasing number of metalloproteins with polymetallic active sites.[1] In another area of research, there is an intensive effort to design and understand new "molecular magnets",[2,3] which is mainly directed toward the development of new materials with novel electronic properties. Thus the study of metal−metal interactions between paramagnetic metal centers through multiatom bridges has been one of the most active research fields in inorganic chemistry with the aim of understanding fundamental factors governing the exchange interactions.

Both homo- and heteropolymetallic systems provide opportunity to study different fundamental electronic processes. New exchange pathways can be expected for heteropolynuclear complexes,[3,4] where unusual sets of magnetic orbitals can be made to overlap with each other; hence investigations of a series of heteropolynuclear complexes might be more informative in comparison to those of homopolynuclear complexes. It is worth mentioning in this connection that the presence of different competing interactions owing to the topologies in polynuclear complexes may lead to ground and other low-lying states that cannot be expected by simple combination of the local spins according to the nature of the interactions present between the spin carriers. We will demonstrate in this paper several examples of such "ground-state variability".[3−5]

The ability of the tris(dimethylglyoximato)metalate(II) tetraanion to act as a bridging ligand to form both homo- and heterometallic complexes with iron(III)[6,7] being the terminal metal ion has allowed us to investigate the novel properties of a number of linear heterotrinuclear complexes. These dimethylglyoximato-bridged linear trinuclear complexes of general formula $[LFe^{III}\{(\mu\text{-dmg})_3M^{II}\}Fe^{III}L]^{2+}$, where $M^{II} = Zn^{II}$, Cu^{II},

[†] Max-Planck-Institut für Strahlenchemie.
[‡] Universität-Gesamthochschule Paderborn.
[§] Medizinische Universität zu Lübeck.

(1) See for example: (a) Holm, R. H., Solomon, E. I. Guest Eds. *Chem. Rev.* **1996**, *96*, No. 7. (b) Feig, A. L.; Lippard, S. J. *Chem. Rev.* **1994**, *94*, 759. (c) Kurtz, D. M. *Chem. Rev.* **1990**, *90*, 585. (d) Que, L.; True, A. E. *Prog. Inorg. Chem.* **1990**, *38*, 98.
(2) (a) *Magnetic Molecular Materials*; Gatteschi, D., Kahn, O., Miller, J. S., Palacio, F., Eds.; NATO ASI Series E, Vol. 198; Kluwer Academic: Dordrecht, The Netherlands, 1990. (b) Kahn, O. *Molecular Magnetism;* VCH Verlagsgesellschaft: Weinheim, Germany, 1993.
(3) Kahn, O. *Adv. Inorg. Chem.* **1995**, *43*, 179.
(4) Murray, K. S. *Adv. Inorg. Chem.* **1995**, *43*, 261.
(5) Hendrickson, D. N. In *Research Frontiers in Magnetochemistry*; O'Connor, C. J., Ed.; World Scientific: Singapore, 1993; p 87.

S0020-1669(97)00362-5 CCC: $15.00
Published on Web 04/01/1998

Ni^{II}, Fe^{II}, or Mn^{II}, have been prepared by stepwise reactions of the LFe unit with in situ prepared $[M^{II}(dmg)_3]^{4-}$ ions, where L represents the simple tridentate cyclic amine 1,4,7-trimethyl-1,4,7-triazacyclononane, which coordinates facially in octahedral complexes.

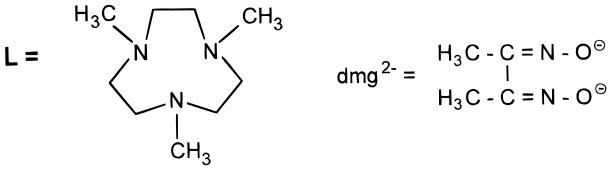

In this paper, we explore the effects of replacing Fe(III) with either Mn(III) or Mn(IV), which are quasi-isostructural but not isoelectronic with the $Fe^{III}M^{II}Fe^{III}$ centers. We report the syntheses and magnetic and spectroscopic properties of the complexes $[LMn^{III}\{(\mu\text{-dmg})_3M^{II}\}Mn^{III}L](ClO_4)_2$, where M^{II} = Mn^{II} (**1**), Ni^{II} (**2**), Cu^{II} (**3**), or Zn^{II} (**4**), and $[LMn^{IV}\{(\mu\text{-dmg})_3M^{II}\}Mn^{IV}L](ClO_4)_4$, where M^{II} = Mn^{II} (**5**), Ni^{II} (**6**) Cu^{II} (**7**), or Zn^{II} (**8**), together with the crystal structures of Mn^{III}-$Mn^{II}Mn^{III}$, **1**, and $Mn^{III}Cu^{II}Mn^{III}$, **3**. Throughout this paper, the compounds are denoted by the metal centers only; the macrocyclic amine and the oxime ligands are omitted for clarity.

Experimental Section

The macrocycle 1,4,7-trimethyl-1,4,7-triazacyclononane ($L = C_9H_{21}N_3$) was prepared as described previously.[8] All other starting materials were commercially available and were of reagent grade. Elemental analyses (C, H, N) were performed by the Microanalytical Laboratory, Ruhr Universität Bochum. Manganese was determined spectrophotometrically by using pyridine-2,6-dicarboxylic acid;[9] copper and nickel were determined gravimetrically by using *N*-benzoyl-*N*-phenylhydroxylamine and dimethylglyoxime, respectively. Zinc was determined by atomic absorption spectrometry. The perchlorate anion was determined gravimetrically as tetraphenylarsonium perchlorate. Electronic absorption spectra were measured on a Perkin-Elmer Lambda 9 spectrophotometer in solution. Fourier transform infrared spectroscopy on KBr pellets was performed on a Perkin-Elmer 1720X FT-IR instrument.

Cyclic voltammetric experiments were performed with a Princeton Applied Research model 173 potentiostat−galvanostat driven by a model 175 universal programmer, and details of the experimental procedure have been described earlier.[7]

Magnetic susceptibilities of powdered samples were recorded on a SQUID magnetometer (MPMS, Quantum Design) in the temperature range 2−295 K with an applied field of 1 T. Experimental susceptibility data were corrected for the underlying diamagnetism using Pascal's constants.

The X-band EPR spectra of the polycrystalline material either as solid or in solution were recorded at various temperatures between 3 and 100 K with a Bruker ER 200 D-SRC spectrometer equipped with a standard TE 102 cavity, an Oxford Instruments liquid helium continuous-flow cryostat, an NMR gaussmeter, a frequency meter, and a data acquisition system (our own development).

Syntheses of the Compounds. (a) $[LMn^{III}\{(\mu\text{-dmg})_3Mn^{II}\}Mn^{III}L](ClO_4)_2$ (1). Manganese(III) acetate dihydrate (0.27 g, 1 mmol) was added to a deaerated solution of 1,4,7-trimethyl-1,4,7-triazacyclononane (0.17 g, 1 mmol) in 40 mL of methanol under vigorous stirring. The resulting red-brown solution was charged with solid samples of $Mn(CH_3COO)_2\cdot 4H_2O$ (0.12 g, 0.5 mmol), dimethylglyoxime (0.17 g, 1.5 mmol), and sodium methoxide (0.27 g, 5 mmol). The suspension was stirred under argon at room temperature for 2 h, until a dark brown solution was obtained. The solution was filtered to remove any solid particles. Sodium perchlorate monohydrate (0.4 g) was added, and the dark brown solution was kept at 4 °C. After 24 h, dark red-brown needles were collected by filtration and air-dried. One of these crystals was used in the structural characterization of the complex. Yield: 0.21 g (∼40%). Anal. Calcd for $[C_{30}H_{60}N_{12}O_6Mn_3](ClO_4)_2$: C, 34.36; H, 5.77; N, 16.03; Mn, 15.7; ClO_4, 18.97. Found: C, 35.5; H, 5.7; N, 15.9; Mn, 15.2; ClO_4, 19.3. IR (KBr, cm^{-1}): ν(CN) 1582 m, ν(NO) 1182 m. UV−vis in CH_3OH [λ_{max}, nm (ϵ, $M^{-1}\,cm^{-1}$)]: 280 (28 800), 314 sh (25 200), 522 (1710).

(b) $[LMn^{III}\{(\mu\text{-dmg})_3Ni^{II}\}Mn^{III}L](ClO_4)_2$ (2). All operations were done under an argon atmosphere. To a rapidly stirred and degassed solution of 1,4,7-trimethyl-1,4,7-triazacyclononane (0.17 g, 1 mmol) in 40 mL of methanol was added a sample of 0.27 g of manganese(III) acetate.

Stirring was continued further until a clear red-brown solution was obtained. A sample of 0.17 g (1.5 mmol) of dimethylglyoxime and 1 mL of triethylamine were added. To this suspension was added dropwise a solution (10 mL) of $NiCl_2\cdot 6H_2O$ (0.12 g, 0.5 mmol) in methanol over a period of 0.5 h. The suspension was refluxed for 2 h and then filtered to remove precipitated $Ni(dmgH)_2$. Sodium perchlorate hydrate (0.4 g) was added, and the dark-brown solution on cooling at 4 °C for 24 h afforded brown needles, which were collected by filtration and air-dried. Yield: 0.15 g (∼29%). Anal. Calcd for $[C_{30}H_{60}N_{12}O_6Mn_2Ni](ClO_4)_2$: C, 34.24; H, 5.75; N, 15.97; Mn, 10.44; Ni, 5.58; ClO_4, 18.90. Found: C, 33.8; H, 5.6; N, 15.9; Mn, 10.3; Ni, 5.3; ClO_4, 19.1. IR (KBr, cm^{-1}): ν(CN) 1588 m, ν(NO) 1187 m, 1212 m. UV−vis in CH_3OH [λ_{max}, nm (ϵ, $M^{-1}\,cm^{-1}$)]: 273 (32 760), 550 sh (2060).

(c) $[LMn^{III}\{(\mu\text{-dmg})_3Cu^{II}\}Mn^{III}L](ClO_4)_2$ (3). A solution of the cyclic amine (0.17 g, 1 mmol) in 40 mL of methanol under argon was treated with a sample of manganese(III) acetate (0.27 g, 1 mmol) under vigorous stirring in a round-bottomed flask. After 0.25 h of stirring, the resulting red-brown solution was charged with a sample of $Cu(dmgH)_2$ (0.15 g, 0.5 mmol), dimethylglyoxime (0.06 g, 0.5 mmol), and 1 mL of triethylamine. The very dark mixture was stirred for a further 2 h at ambient temperature and filtered to remove the remaining solid $Cu(dmgH)_2$. After addition of $NaClO_4\cdot H_2O$ (0.4 g), the dark solution kept at 4 °C overnight provided brown needles. The crystals were collected by filtration and air-dried. Yield: 0.35 g (∼66%). Anal. Calcd for $[C_{30}H_{60}N_{12}O_6Mn_2Cu](ClO_4)_2$: C, 34.08; H, 5.72; N, 15.90; Mn, 10.39; Cu, 6.01; ClO_4, 18.81. Found: C, 33.6; H, 5.8; N, 15.8; Mn, 10.2; Cu, 5.8; ClO_4, 18.9. IR (KBr, cm^{-1}): ν(CN) 1577 m, 1595 m; ν(NO) 1198 m. UV−vis in CH_3OH [λ_{max}, nm (ϵ, $M^{-1}\,cm^{-1}$)]: 272 (38 700), 435 sh (4650), 580 sh (1200), ∼700 sh (800).

A suitable crystal was selected from the batch for an X-ray diffraction study.

(d) $[LMn^{III}\{(\mu\text{-dmg})_3Zn^{II}\}Mn^{III}L](ClO_4)_2$ (4). Compound **4** was prepared as previously described.[10] IR (KBr, cm^{-1}): ν(CN) 1596 s; ν(NO) 1212. UV−vis in CH_3OH [λ_{max}, nm (ϵ, $M^{-1}\,cm^{-1}$)] 280 sh (29 060), 302 (30 110), 535 sh (920)

(e) $[LMn^{IV}\{(\mu\text{-dmg})_3M^{II}\}Mn^{IV}L](ClO_4)_4$, Where M^{II} = Mn^{II} (5), Ni^{II} (6), Cu^{II} (7), or Zn^{II} (8). Because **5**−**8** were prepared very similarly, a representative method only is described. An argon-scrubbed solution of **1**, **2**, **3**, or **4** (100 mg) in CH_3CN (40 mL) was stirred with 30 mg of $NOBF_4$ for 0.5 h. After addition of $NaClO_4$ (0.1 g) and on cooling at −10 °C for 12 h, dark brown microcrystals were collected by filtration and air-dried. Yield: 80−100 mg (60−80%).

Anal. Calcd for $[C_{30}H_{60}N_{12}O_6Mn_3](ClO_4)_4$ (**5**): C, 28.88; H, 4.85; N, 13.47; Mn, 13.21; ClO_4, 31.89. Found: C, 28.2; H, 4.8; N, 13.3; Mn, 13.1; ClO_4, 31.7. IR (KBr, cm^{-1}): ν(CN) 1596 w; ν(NO) 1212 w. UV−vis in H_2O [λ_{max}, nm (ϵ, $M^{-1}\,cm^{-1}$)]: 225 (44 100), 280 sh (17 000), ∼460 sh (1000), 825 sh (80), 961 (90), 1155 (120).

Anal. Calcd for $[C_{30}H_{60}N_{12}O_6Mn_2Ni](ClO_4)_4$ (**6**): C, 28.79; H, 4.83; N, 13.43; Mn, 8.78; Ni, 4.69; ClO_4, 31.79. Found: C, 28.5; H, 4.7; N, 13.4; Mn, 8.2; Ni, 4.8; ClO_4, 31.1. IR (KBr, cm^{-1}): ν(CN) 1605

(6) Chaudhuri, P.; Winter, M.; Fleischhauer, P.; Haase, W.; Flörke, U.; Haupt, H.-J. *J. Chem. Soc., Chem. Commun.* **1990**, 1728.
(7) Chaudhuri, P.; Winter, M.; Della Vedova, B. P. C.; Fleischhauer, P.; Haase, W.; Flörke, U.; Haupt, H.-J. *Inorg. Chem.* **1991**, *30*, 4777.
(8) Wieghardt, K.; Chaudhuri, P.; Nuber, B.; Weiss, J. *Inorg. Chem.* **1982**, *21*, 3086.
(9) Hartkamp, H. *Z. Anal. Chem.* **1964**, *199*, 183.
(10) Chaudhuri, P.; Winter, M.; Birkelbach, F.; Fleischhauer, P.; Haase, W.; Flörke, U.; Haupt, H.-J. *Inorg. Chem.* **1991**, *30*, 4291.

Table 1. Crystallographic Data for $[L_2Mn^{III}_2(dmg)_3Mn^{II}](ClO_4)_2$, **1**, and $[L_2Mn^{III}_2(dmg)_3Cu^{II}](ClO_4)_2$, **3**

	$Mn^{III}_2Mn^{II}$, **1**	$Mn^{III}_2Cu^{II}$, **3**
empirical formula	$C_{30}H_{60}Cl_2N_{12}O_{14}Mn_3$	$C_{30}H_{60}Cl_2N_{12}O_{14}Mn_2Cu$
fw	1048.6	1057.2
crystal size, mm	0.06 × 0.43 × 0.29	0.27 × 0.30 × 0.44
color, habit	brown-red needle	dark brown needle
crystal system	monoclinic	monoclinic
space group	*C*2/*c*	*C*2/*c*
a, Å	32.472(6)	32.686(5)
b, Å	9.058(2)	8.870(1)
c, Å	16.729(3)	16.867(2)
β, deg	107.60(3)	108.65(1)
V, Å^3	4690(2)	4633(1)
Z	4	4
D_{calcd}, g cm^{-3}	1.485	1.516
λ(Mo Kα), Å	0.710 73	0.710 73
diffractometer	Siemens P4	Siemens R3m/V
μ, mm^{-1}	0.946	1.18
2θ limits, deg	$3 \le 2\theta \le 50.0$	$3 \le 2\theta \le 55.0$
no. of reflns with $F > 4\sigma(F)$	1305	3634
F(000)	2180	2196
T, K	293	293
R[a]	9.07	4.8

[a] For $I > 2\sigma(I)$; $R = \sum||F_o| - |F_c||/\sum|F_o|$.

w; ν(NO) 1156, 1212 w. UV−vis in H_2O [λ_{max}, nm (ϵ, M^{-1} cm^{-1})]: 232 (29 400), 272 (32 400), 335 sh (26 000), 450 sh (11 200), ∼550 sh (8000).

Anal. Calcd for $[C_{30}H_{60}N_{12}O_6Mn_2Cu](ClO_4)_4$ (**7**): C, 28.69; H, 4.81; N, 13.38; Mn, 8.75; Cu, 5.06; ClO_4, 31.67. Found: C, 28.6; H, 4.8; N, 12.8; Mn, 8.5; Cu, 5.2; ClO_4, 30.7. IR (KBr, cm^{-1}): ν(CN) 1601 w; ν(NO) 1212 w. UV−vis in H_2O [λ_{max}, nm (ϵ, M^{-1} cm^{-1})]: 257 (32 800), 284 (33 290), 380 sh (18 300), 450 sh (14 500).

$[C_{30}H_{60}N_{12}O_6Mn_2Zn](ClO_4)_4$ (**8**) has been described in an earlier publication.[10] IR (KBr, cm^{-1}): ν(CN) 1616 m; ν(NO) 1212 w. UV−vis in H_2O [λ_{max}, nm (ϵ, M^{-1} cm^{-1})] 266 (33 500), 310 sh (25 600), 401 (29 900).

5−**8** could also be obtained in the form of crystalline hexagonal plates by slowly diffusing a solution of tetrabutylammonium peroxodisulfate in acetonitrile into solutions of the corresponding Mn(III)-containing trinuclear complexes through a glass frit (G4) in a closed two-compartment glass apparatus.

Caution! Although we experienced no difficulties with the compounds isolated as their perchlorate salts, the unpredictable behavior of perchlorate salts necessitates extreme caution in their handling.

Crystal Structure Determinations. Diffraction data for **1** were obtained on a Siemens P4 diffractometer, using graphite-monochromatized Mo Kα radiation at 293 K. Pertinent crystallographic parameters are summarized in Table 1. The data were corrected for Lorentz and polarization effects, but it was not necessary to account for crystal decay. An empirical absorption correction based on ψ scans was applied.[11] The scattering factors[12] for neutral non-hydrogen atoms were corrected for both the real and the imaginary components of anomalous dispersion. The structure of **1** was determined by direct methods (SHELXTL PLUS). The structure was refined by a full-matrix least-squares technique; the function minimized was $\sum w(F_o - F_c)^2$ where $1/w = \sigma^2(F) + 0.0008F^2$. Idealized positions of H atoms bound to carbon atoms were calculated (C−H = 0.96 Å) and included in the refinement cycle.

A dark brown crystal of the trinuclear complex $Mn^{III}_2Cu^{II}$, **3**, with dimensions 0.27 × 0.30 × 0.44 mm was mounted on a Siemens R3m/V diffractometer. Preliminary examinations showed that the crystal belonged to the monoclinic crystal system, space group *C*2/*c*. The lattice parameters were obtained at 20 °C by a least-squares refinement of the angular settings ($14° \le 2\theta \le 30°$) of 30 reflections. The data are summarized in Table 1. A total of 5353 intensities were collected using $\omega-2\theta$ scans in the ranges $3 \le 2\theta \le 55°$, $-42 \le h \le 42$, $0 \le k \le 11$, $0 \le l \le 21$. Three standard reflections monitored every 400 measurements showed only random deviations. An Lp correction and an empirical absorption correction (ψ scans) were applied. The structure of **3** was solved by comparison of cell constants with those of the isotypic $Mn^{III}_2Zn^{II}$ complex[10] using atomic parameters of the latter as starting parameters for full-matrix least-squares refinement (SHELXTL V5), based on F^2 with 287 parameters. All but H atoms were refined anisotropically. H atoms were treated with a "riding model" at idealized positions. Displacement parameters of O(14) indicate some degree of orientational disorder of the ClO_4 group. Cu was refined with a split model with site occupations 0.391 for Cu(1) and 0.109 for Cu(2). Cu without a split model lies on a special site with site symmetry 2 (i.e., site occupation factor 0.5); the split-position Cu(1) lies on a special site too, and Cu(2) lies on a general position. Selected interatomic distances and angles are given in Tables 2 and 3 for the $Mn^{III}_2Mn^{II}$, **1**, and the $Mn^{III}_2Cu^{II}$, **3**, compounds, respectively.

Table 2. Selected Bond Lengths (Å) and Angles (deg) for $[L_2Mn_2(dmg)_3Mn](ClO_4)_2$ **1**

Mn(2)−Mn(1)−Mn(2a)	179.2(2)		
Mn(2)···Mn(1)	3.571(1)	Mn(2)···Mn(2a)	7.141(2)
Mn(1)−N(1)	2.194(15)	Mn(1)−N(2)	2.205(19)
Mn(1)−N(3)	2.202(18)	Mn(1)−N(1a)	2.194(15)
Mn(1)−N(2a)	2.205(19)	Mn(1)−N(3a)	2.202(18)
Mn(2)−O(1)	1.961(15)	Mn(2)−O(2)	1.994(12)
Mn(2)−O(3)	1.947(14)	Mn(2)−N(4)	2.182(23)
Mn(2)−N(5)	2.106(17)	Mn(2)−N(6)	2.149(18)
O(1)−N(1)	1.375(22)	O(2)−N(2)	1.350(20)
O(3)−N(3)	1.376(21)	N(1)−C(1)	1.265(30)
N(2)−C(3)	1.214(25)	N(3)−C(5)	1.295(28)
N(1)−Mn(1)−N(2)	89.8(6)	N(1)−Mn(1)−N(3)	88.0(6)
N(2)−Mn(1)−N(3)	89.2(7)	N(1)−Mn(1)−N(1a)	129.2(9)
N(2)−Mn(1)−N(1a)	71.8(6)	N(3)−Mn(1)−N(1a)	136.5(7)
N(1)−Mn(1)−N(2a)	71.8(6)	N(2)−Mn(1)−N(2a)	136.8(8)
N(3)−Mn(1)−N(2a)	127.3(7)	N(1a)−Mn(1)−N(2a)	89.8(6)
N(1)−Mn(1)−N(3a)	136.5(7)	N(2)−Mn(1)−N(3a)	127.3(7)
N(3)−Mn(1)−N(3a)	72.7(9)	N(1a)−Mn(1)−N(3a)	88.0(6)
N(2a)−Mn(1)−N(3a)	89.2(7)	O(1)−Mn(2)−O(2)	99.3(5)
O(1)−Mn(2)−O(3)	99.1(7)	O(2)−Mn(2)−O(3)	101.2(6)
O(1)−Mn(2)−N(4)	166.5(6)	O(2)−Mn(2)−N(4)	90.7(7)
O(3)−Mn(2)−N(4)	87.8(7)	O(1)−Mn(2)−N(5)	88.8(7)
O(2)−Mn(2)−N(5)	166.6(7)	O(3)−Mn(2)−N(5)	88.0(7)
N(4)−Mn(2)−N(5)	79.8(8)	O(1)−Mn(2)−N(6)	90.8(7)
O(2)−Mn(2)−N(6)	89.9(6)	O(3)−Mn(2)−N(6)	163.6(6)
N(4)−Mn(2)−N(6)	80.0(8)	N(5)−Mn(2)−N(6)	79.2(7)

Results and Discussion

Preparation and Characterization of Complexes. The red-brown solution obtained from manganese(III) acetate and the cyclic amine (L) in methanol reacting with M^{2+} and dmg^{2-} ions, prepared in situ, affords in the presence of a counterion, e.g. ClO_4^-, dark brown crystals of $[L_2Mn^{III}_2(dmg)_3M^{II}](ClO_4)_2$ (M = Mn (**1**), Ni (**2**), Cu (**3**), Zn (**4**)). The purpose of added triethylamine or sodium methoxide is to provide a basic medium needed for the deprotonation of the O···H···O groups[13] present in mainly solid $M^{II}(dmgH)_2$. The presumably dianionic $M(dmg)_2^{2-}$ species produced in this way can now react with the (μ-oxo)bis(μ-acetato)manganese(III) species, prepared in situ in the aforementioned red-brown solution, to produce a $Mn^{III}_2(dmg)_2M^{II}$ species which subsequently adds an dianionic dmg^{2-} ligand to form the $Mn^{III}_2(dmg)_3M^{II}$ species. The comparatively low yield for the preparation of the $Mn^{III}Ni^{II}Mn^{III}$ complex is a result of low concentration of $Ni(dmg)_2^{2-}$ ion in the solution,

(11) SHELXTL-PLUS program package (PC Version) by G. M. Sheldrick, Universität Göttingen.
(12) *International Tables for X-ray Crystallography*; Kynoch: Birmingham, England, 1974; Vol. 4.
(13) (a) Blinc, R.; Hadzi, D. *J. Chem. Soc. A* **1958**, 4536 (b) Burger, K.; Ruff, F. *J. Inorg. Nucl. Chem.* **1965**, *27*, 179. (c) Caton, J. E.; Banks, E. V. *Inorg. Chem.* **1967**, *6*, 1670.

Table 3. Selected Bond Distances (Å) and Angles (deg) for $[L_2Mn_2Cu(dmg)_3](ClO_4)_2$ **3**[a]

	Mn−Cu−Mn	167.3(3)	
Cu···Mn	3.578(1)	Mn···Mn	7.111(2)
Cu(1)−N(1)	2.043(4)	Cu(1)−N(2)	2.029(3)
Cu(1)−N(3)	2.354(5)	Mn−O(1)	1.965(2)
Mn−O(2)	2.028(2)	Mn−O(3)	1.899(2)
Mn−N(4)	2.174(3)	Mn−N(5)	2.231(3)
Mn−N(6)	2.127(3)	O(1)−N(1)	1.355(3)
O(2)−N(2)	1.348(3)	O(3)−N(3)	1.368(3)
N(1)−C(1)	1.286(4)	N(2)−C(3)	1.283(4)
N(3)−C(5)	1.270(4)		
N(1)−Cu(1)−N(1A)	143.6(2)	N(1)−Cu(1)−N(2)	95.9(1)
N(1)−Cu(1)−N(2A)	78.3(1)	N(1)−Cu(1)−N(3)	82.6(1)
N(1)−Cu(1)−N(3A)	131.1(2)	N(2)−Cu(1)−N(2A)	161.7(2)
N(2)−Cu(1)−N(3)	82.5(1)	N(2)−Cu(1)−N(3A)	113.5(1)
N(3)−Cu(1)−N(3A)	64.8(2)	O(1)−Mn−O(2)	96.6(1)
O(1)−Mn−O(3)	96.9(1)	O(1)−Mn−N(4)	169.1(1)
O(1)−Mn−N(5)	91.2(1)	O(1)−Mn−N(6)	90.9(1)
O(2)−Mn−O(3)	99.6(1)	O(2)−Mn−N(4)	91.3(1)
O(2)−Mn−N(5)	167.3(1)	O(2)−Mn−N(6)	89.1(1)
O(3)−Mn−N(4)	89.2(1)	O(3)−Mn−N(5)	89.4(1)
O(3)−Mn−N(6)	167.5(1)	N(4)−Mn−N(5)	79.8(1)
N(4)−Mn−N(6)	81.6(4)	N(5)−Mn−N(6)	80.7(1)

[a] Similar bond lengths and angles for Cu(2).

as is evidenced by the precipitation of a major part of the Ni^{2+} ions as $Ni(dmgH)_2$. As anticipated, the trinuclear complexes $Mn^{III}M^{II}Mn^{III}$ are amenable to oxidation (loc. cit.) and give rise to $Mn^{IV}M^{II}Mn^{IV}$ species (M = Mn (**5**), Ni (**6**), Cu (**7**), Zn (**8**)) when oxidized in acetonitrile with NO^+ or $S_2O_8^{2-}$ as an oxidant. The same species can also be obtained by electrochemical oxidation. Complexes **1**−**4** are sparingly soluble in water with decomposition but reasonably soluble in organic solvents such as acetone, alcohols, and acetonitrile. Complexes **5**−**8** are hardly soluble in common organic solvents but are readily soluble in water.

The optical spectra of **1**−**4** in methanol and of **5**−**8** in water at ambient temperature have been measured in the 200−1200 nm wavelength range (see Experimental Section). On the basis of high extinction coefficients and the relative sharpness of the bands, most of the bands can be ascribed to either charge-transfer transitions within the ligands or metal-to-ligand charge transfer (MLCT). The bands at ∼700 nm for **3**, 535 nm for **4**, and 961 and 1155 nm for **5** are thought to be due to ligand field (d−d) transitions. The extinction coefficients of these bands are large in comparison to those for the 6-coordinated transition metal complexes, probably because of the intensity gain through exchange coupling[14] and of the strong trigonal distortion (D_3)[15] of the metal centers.

The presence or absence of certain bands in the generally complicated IR spectra has been utilized to establish the nature of the complexes. The medium-strong bands at 1186−1212 cm^{-1} are assignable to the NO stretching vibration.[13] The second NO infrared absorption could not be observed in the perchlorate salts **1**−**8**, because of the superposition of the strong band originating from the perchlorate anions. The ν(CN) vibrations of the complexes containing the trivalent manganese ions are situated at a significantly lower frequency than those for the corresponding tetravalent manganese ions, where these vibrations are found at 1577−1596 cm^{-1} for Mn(III) and 1596−1616 cm^{-1} for Mn(IV) (see Experimental Section).

Description of the Structures. (a) Molecular Structure of $[L_2Mn^{III}_2\{(\mu\text{-dmg})_3Mn^{II}\}(ClO_4)_2$ (1). The molecular geometry and the atom-labeling scheme of the cation in **1** are shown in Figure 1. The structure of the complex cation consists of a discrete dicationic trinuclear unit having a crystallographic 2-fold symmetry and two noncoordinatively bound perchlorate anions. Selected bond lengths and angles are listed in Table 2. The X-ray structure confirms that a linear trinuclear complex (Mn(2)−Mn(1)−Mn(2a) = 179.2°) has indeed been formed in such a way that a trioctahedral geometry containing a manganese(II) and two manganese(III) as central atoms is present in the lattice. The central tris(dimethylglyoximato)manganate(II) ion, $[Mn(dmg)_3]^{4-}$, bridges the two terminal manganese(III) centers through the deprotonated oxime oxygens. The terminal manganese coordination geometry is distorted octahedral with three nitrogen atoms from the facially coordinated tridentate macrocyclic amine and three oxygen atoms from three bridging oximate groups. The central MnN_6 core is nearly trigonal prismatic. The six imine nitrogen atoms are arranged around the Mn(II) center with a twist angle of 5.7° between the triangular faces comprising N(1)N(2)N(3) and N(1a)N(2a)N(3a) atoms. An intramolecular Mn(2)···Mn(2a) separation of 7.141(2) Å has been found. The nearest neighbor Mn(2)···Mn(1) distance within the trinuclear cation is 3.571 Å. The average Mn(III)−N, 2.146(3) Å, and Mn(III)−O, 1.967(3) Å, bond lengths are similar to those of the analogous $[L_2Mn_2(dmg)_3Zn]^{2+}$ complex.[10] The largest deviation from idealized 90° interbond angles is 11°, which occurs within the five-membered C−C−N−Mn(2)−N chelate rings, the N−Mn(2)−N angles ranging between 79.2(7) and 80.0(8)°, whereas the O−Mn(2)−O angles fall between 99.1(7) and 101.2(6)°. The bond lengths are consistent with a d^4 high-spin electron configuration for the terminal Mn(III) centers.[16]

The average Mn(1)−N(oxime) distance, 2.200(5) Å, is shorter than those found in comparable high-spin Mn(II)−N(oxime)[17] structures, 2.285(10) and 2.366(20) Å, but appreciablly longer than those found in low-spin Mn(II)−N(oxime) structures, 1.95 Å.[18] The usual coordination number of Mn(II) is 6, and since high-spin Mn(II) obtains no ligand field stabilization in either an octahedral or a tetrahedral environment, the geometry around the Mn(1) is dictated by the ligand constraints. In this case, we observe a six-coordinate complex with close to trigonal geometry.

Although the N−O (average 1.367(15) Å) bond lengths and the C−N−O (average 117.8(11)°) bond angles of the bridging dimethylglyoximato ligands are comparable to the corresponding metrical parameters of other comparable structures, the C═N bond lengths differ remarkably from each other, varying from 1.214(25) to 1.295(28) Å.

(b) Molecular Structure of $[L_2Mn^{III}_2\{(\mu\text{-dmg})_3Cu^{II}\}](ClO_4)_2$ (3). The X-ray structure of the cation in **3** clearly illustrates the trinuclear nature of this complex. The cation together with the atom-labeling scheme used is shown in Figure 2. Selected bond lengths and angles are listed in Table 3. The $[Cu(dmg)_3]^{4-}$ anion bridges two terminal manganese(III) ions through its deprotonated oxime oxygens with a Mn···Cu separation of 3.578(1) Å. The trinuclear Mn−Cu−Mn angle

(14) McCarthy, P. J.; Gudel, H. V. *Coord. Chem. Rev.* **1988**, *88*, 69.
(15) Lever, A. B. P. *Inorganic Electronic Spectroscopy*; Elsevier: Amsterdam, 1984.
(16) Wieghardt, K. *Angew. Chem.* **1989**, *101*, 1179; *Angew. Chem., Int. Ed. Engl.* **1989**, *28*, 1153.
(17) Jurisson, S.; Francesconi, L.; Linder, K. E.; Treher, E.; Malley, M. F.; Gougoutas, J. Z.; Nunn, A. D. *Inorg. Chem.* **1991**, *30*, 1820.
(18) (a) Chattopadhyay, S.; Basu, P.; Pal, S.; Chakravorty, A. *J. Chem. Soc., Dalton Trans.* **1990**, 3829. (b) Basu, P.; Chakravorty, A. *Inorg. Chem.* **1992**, *31*, 4980.

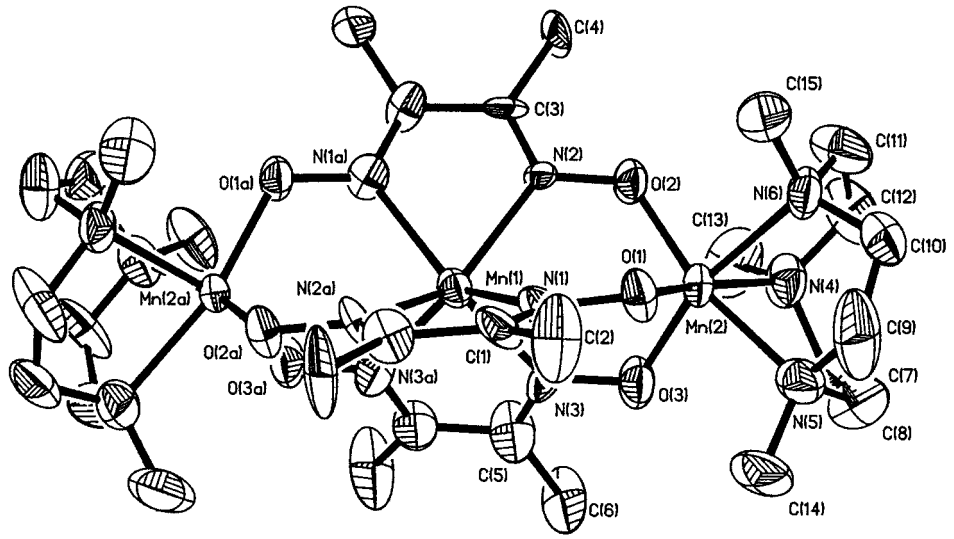

Figure 1. ORTEP view of the trinuclear $Mn^{III}Mn^{II}Mn^{III}$ cation in **1**.

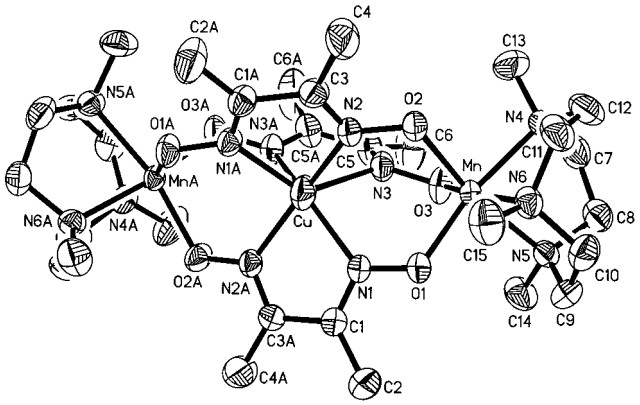

Figure 2. Molecular structure of the trinuclear $Mn^{III}Cu^{II}Mn^{III}$ cation in **3**, showing only one Cu position.

is 167.3°, with a Mn···Mn separation of 7.11 Å. The nearest *inter*molecular Mn(III)···Mn(III) separation is 8.451(1) Å. Two facially coordinated tridentate amine ligands complete the trigonally distorted octahedral coordination sphere of the two Mn(III) centers. The Mn−O and Mn−N distances are consistent with a d^4 high-spin electron configuration of the terminal manganese centers and are comparable with those in **1**.

The Cu−N distances and the twist angles show that the resultant coordination sphere around the disordered Cu is strongly distorted. The six imine nitrogen atoms are arranged around the Cu(II) center with two different twist angles of 10.7 and 12.3° between the triangular faces comprising the oxime nitrogens. The Cu atom is thus displaced from the center of the complex and closer to two of the bridging dimethyloximate ligands; the distance to the third oxime ligand is remarkably long. The geometry of the Cu center may be envisaged as pseudo-square-pyramidal, with an η^2-dmg ligand at the apical position, and is very similar to that found in the corresponding $Fe^{III}Cu^{II}Fe^{III}$ compound.[6]

The molecular structure of $Mn^{III}Zn^{II}Mn^{III}$, **4**, has been reported earlier.[10]

Electrochemistry. The cyclic voltammogram of $Mn^{III}Mn^{II}$-Mn^{III}, **1**, at ambient temperature in CH_3CN containing 0.1 M tetra-*n*-butylammonium hexafluorophosphate as supporting electrolyte at a platinum-button working electrode with a scan rate of 200 mV s^{-1} is shown in Figure 3. Electrochemical data for **1**−**4** are given in Table 4.

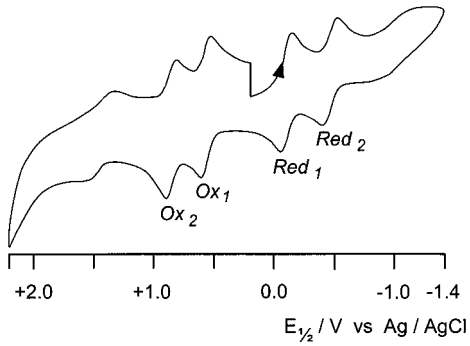

Figure 3. Cyclic voltammogram of **1** in CH_3CN at a scan rate of 0.2 V s^{-1}.

Table 4. Redox Potentials[a] for **1**−**4** Determined by Cyclic Voltammetry

complex	$E_{1/2}(Ox_2)_{rev}$	$E_{1/2}(Ox_1)_{rev}$	$E_{1/2}(Red_1)_{qr}$	$E_{1/2}(Red_2)_{qr}$
$Mn^{III}Mn^{II}Mn^{III}$ (**1**)	0.73	0.44	−0.23	−0.60
$Mn^{III}Ni^{II}Mn^{III}$ (**2**)	0.71	0.47	−0.25	−0.52
$Mn^{III}Cu^{II}Mn^{III}$ (**3**)	0.73	0.43	−0.35	−0.61
$Mn^{III}Zn^{II}Mn^{III}$ (**4**)	0.67	0.43	−0.31	−0.59

[a] V vs NHE; rev = reversible; qr = quasi-reversible.

Two consecutive reversible steps of oxidation in the potential range 0.0−1.0V vs Ag/AgCl are detected for **1**−**4** corresponding to the following electrochemical oxidation processes:

$$Mn^{III}M^{II}Mn^{III} \overset{Ox_1}{\rightleftharpoons} Mn^{IV}M^{II}Mn^{III} \overset{Ox_2}{\rightleftharpoons} Mn^{IV}M^{II}Mn^{IV}$$

That two reversible transfers of one electron per center occur is evident from the adherence to the standard criteria, described in the literature.[19] The reversible character of $E_{1/2}(Ox_1)$ and $E_{1/2}(Ox_2)$ precludes any significant structural rearrangement during the redox processes; i.e., all three species have the same structure in solution and apparently can be described by the solid-state structure as determined by X-ray diffraction of **1**, **3**, and **4**.

Analyses of the cyclic voltammograms in the more negative potential range (0.0 to −1.0V vs Ag/AgCl) with varying scan rates revealed two additional quasi-reversible reduction steps

(19) (a) Nicholson, R. S.; Shain, I. *Anal. Chem.* **1964**, *36*, 706. (b) Bard, A. J.; Faulkner, L. R. *Electrochemical Methods*: *Fundamentals and Applications*; Wiley: New York, 1980.

Table 5. Magnetic Parameters for Homo- and Heterotrinuclear Complexes **1**−**8**

no.	complex	J, cm^{-1} ($J_{12} = J_{23}$)	J_{13}, cm^{-1}	$\langle g \rangle$ ($g_1 = g_2 = g_3$)	D, cm^{-1} (fixed)	ground-state S_t
1	$Mn^{III}Mn^{II}Mn^{III}$	+4.7	−3.0	1.95	D(Mn) = 5.0	$^{13}/_2$, $^{11}/_2$
2	$Mn^{III}Ni^{II}Mn^{III}$	−5.3	+2.7	1.98	D(Mn) = 5.0 D(Ni) = 10.0	3
3	$Mn^{III}Cu^{II}Mn^{III}$	−63.1	−2.8	1.97	D(Mn) = 5.0	$^7/_2$
4	$Mn^{III}Zn^{II}Mn^{III}$		−0.4	2.13		0
5	$Mn^{IV}Mn^{II}Mn^{IV}$	+19.6	−19.2	1.99		$^9/_2$
6	$Mn^{IV}Ni^{II}Mn^{IV}$	+19.2	−10.1	2.10	D(Ni) = 10.0	2, 3
7	$Mn^{IV}Cu^{II}Mn^{IV}$	+72.7	−25.0	2.02		$^3/_2$
8	$Mn^{IV}Zn^{II}Mn^{IV}$		−19.2	2.10		0

attributable to the following equilibria:

$$Mn^{III}M^{II}Mn^{III} \overset{Red_1}{\rightleftharpoons} Mn^{II}M^{II}Mn^{III} \overset{Red_2}{\rightleftharpoons} Mn^{II}M^{II}Mn^{II}$$

Identical cyclic voltammetric behavior has been observed for **5**−**8**.

All attempts to isolate the mixed-valence complexes of either form $Mn^{IV}M^{II}M^{III}$ or the $Mn^{III}M^{II}Mn^{II}$ proved to be unsuccessful. The conproportionation constant K_c for the equilibrium

$$Mn^{III}M^{II}Mn^{III} + Mn^{IV}M^{II}Mn^{IV} \overset{K_c}{\rightleftharpoons} 2Mn^{IV}M^{II}Mn^{III}$$

is calculated to lie in the range 1×10^4 to 1×10^3, which is apparently too low for the isolation of the mixed-valence species.

Magnetic Susceptibility and EPR Studies. The experimental magnetic data in the temperature range 2−295 K of polycrystalline **1**−**8** containing three linearly coupled spins with $J_{12} = J_{23} = J$ and J_{13}, which result from the spin Hamiltonian

$$H = -2J(S_1S_2 + S_2S_3) - 2J_{13}(S_1S_3)$$

for an isotropic exchange coupling with $S_1 = S_3 = 2$ for Mn(III) (compounds **1**−**4**) or $S_1 = S_3 = {}^3/_2$ for Mn(IV) (compounds **5**−**8**) and $S_2 = {}^5/_2$ for Mn(II), **1** and **5**, or $S_2 = 1$ for Ni(II), **2** and **6**, or $S_2 = {}^1/_2$ for Cu(II), **3** and **7**, or $S_2 = 0$ for Zn(II), **4** and **8**, were simulated using a least-squares fitting computer program with a full-matrix diagonalization approach including exchange coupling, Zeeman splitting, and single-ion zero-field interactions (DS_z^2), if necessary. In our model, J ($=J_{12} = J_{23}$) represents the exchange interaction between adjacent metal ions, i.e., the terminal manganese and the central divalent metal ions (J_{12} and J_{23}), whereas J_{13} describes the interaction between the terminal manganese nuclei within the trinuclear complex. Table 5 summarizes the intratrimer exchange parameters together with the observed spin ground states. As the nature of the temperature dependence of the magnetic moments μ_{eff} for **1**−**8** can be immediately seen from Figures 4 and 5, but not easily the exact μ_{eff} values, selected values are listed in Table 6. The solid lines in the Figures 4 and 5 represent the simulations.

To fit particularly the low-temperature data for **1**, it was necessary to consider the single-ion zero-field-splitting parameter for Mn(III), $D(Mn^{III})$, during the fitting procedure. It is important to note that the variations of μ_{eff} are not very sensitive to the sign of D and it is difficult, if not impossible, to determine unambiguously the sign of D from powder magnetic susceptibility measurements. A fixed value of $|D(Mn^{III})|$ at 5.0 cm^{-1} was found to be best suited for the simulation. The nearest-neighbor interaction, J, is ferromagnetic, while J_{13} is antiferromagnetic for **1**. Because of the competing influence of J and J_{13} upon spin coupling in **1**, the ground-state properties are determined by the two, practically degenerate, spin states $^{11}/_2$ and $^{13}/_2$. Similar ground-state variability has been described elsewhere[20]

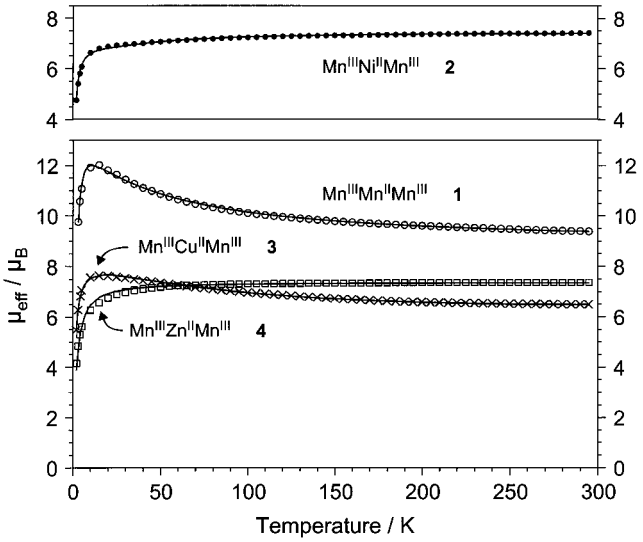

Figure 4. Temperature dependence of the magnetic moments for **1**−**4**. The solid lines represent the best least-squares fits of the experimental data to the Heisenberg−Dirac−van Vleck model.

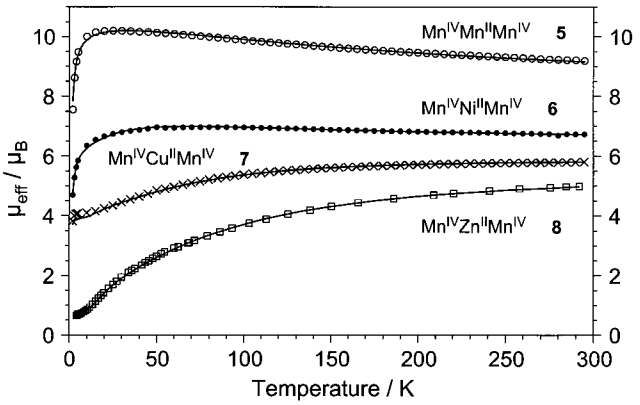

Figure 5. Effective magnetic moment as a function of temperture for **5**−**8**. The solid lines represent the simulation with the spin Hamiltonian (see text).

and will be discussed below in detail for the case of compound **5** with the $Mn^{IV}Mn^{II}Mn^{IV}$ center.

Simulation of the experimental data for **5** yields two coupling constants of nearly the same magnitude, but with opposite signs. The nearest-neighbor coupling, i.e., the exchange interaction between Mn^{IV} and Mn^{II} ions, J, is of ferromagnetic nature with a value of +19.6 cm^{-1}, but the spin interaction between the

(20) (a) McCusker, J. K.; Schmitt, E. A.; Hendrickson, D. N. In *Magnetic Molecular Materials*; Gatteschi, D., Kahn, O., Miller, J. S., Palacio, F., Eds.; NATO ASI Series E, Vol. 198; Kluwer Academic: Dordrecht, The Netherlands, 1990; p 297. (b) Gatteschi, D. *Adv. Mater.* **1994**, *6*, 635. (c) Goodyear, G.; Stratt, R. M. *J. Am. Chem. Soc.* **1993**, *115*, 10452.

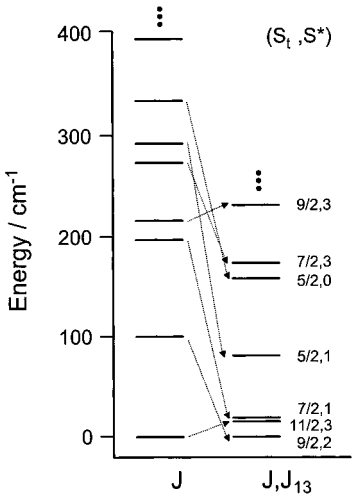

Figure 6. Low-lying spin ladder appropriate for **5** using J and J_{13} (levels on the right) and only J to show the effect of J_{13} on the energy-splitting pattern. The corresponding change in the energy levels of the different states has been denoted by dotted arrows. The energy of the ground state $|S_t, S^*\rangle$ has arbitrarily been set at 0 cm^{-1}.

Table 6. Selective μ_{eff} Values as a Function of Temperature for **1**−**8**

no.	complex	μ_{eff}, μ_B (T, K)
1	$Mn^{III}Mn^{II}Mn^{III}$	9.67 (3), 12.02 (15), 9.39 (295)
2	$Mn^{III}Ni^{II}Mn^{III}$	4.77 (2), 7.15 (70), 7.43 (295)
3	$Mn^{III}Cu^{II}Mn^{III}$	5.48 (2), 7.64 (15), 6.48 (295)
4	$Mn^{III}Zn^{II}Mn^{III}$	4.14 (2), 6.74 (20), 7.36 (295)
5	$Mn^{IV}Mn^{II}Mn^{IV}$	7.56 (2), 10.20 (35−20), 9.19 (295)
6	$Mn^{IV}Ni^{II}Mn^{IV}$	4.70 (2), 6.97 (50), 6.73 (295)
7	$Mn^{IV}Cu^{II}Mn^{IV}$	3.81 (2), 5.79 (295)
8	$Mn^{IV}Zn^{II}Mn^{IV}$	0.64 (4.1), 4.98 (292)

terminal Mn(IV) ions is antiferromagnetic with $J_{13} = -19.2$ cm^{-1}. This relatively strong coupling, considering the long distance of ∼7.1 Å between the terminal manganese centers, has a profound influence on the structure of the spin ladder yielding a ground state with $S_t = {}^9/_2$, which lies 17.2 cm^{-1} below the first excited state with $S_t = {}^{11}/_2$. Neglecting the terminal coupling the ground state of **5** would be $S_t = {}^{11}/_2$. This situation is depicted in Figure 6. The energy ladder obtained from the susceptibility data are further verified by the isothermal magnetization measurements at 5 K in applied fields up to 5 T. The data as squares are shown in Figure 7. The solid line represents the theoretical magnetization behavior of $S = {}^9/_2$ with $g = 1.97$ and is calculated from the expression

$$M = \frac{NgS}{kT}\left\{\frac{2S+1}{2S}\coth\left[\frac{S(2S+1)}{2S}x\right] - \frac{1}{2S}\coth\left[\frac{x}{2}\right]\right\}$$

where $x = g\mu_B B/kT$. The dashed lines in Figure 7 represent the theoretical magnetization curves for $S = {}^7/_2$ and ${}^{11}/_2$. Figure 7 clearly shows that the lowest lying state for **5** is $S_t = {}^9/_2$, owing its origin to the two competing exchange interactions J and J_{13}.

The μ_{eff} values for **2**, $Mn^{III}Ni^{II}Mn^{III}$ (Figure 4), vary only slightly over the temperature range 295−70 K. The low-temperature behavior of **2** is attributed to the zero-field splitting. The parameters used for the least-squares fitting, shown as a solid line in Figure 4, of the experimental data are $J = -5.3$ cm^{-1}, $J_{13} = +2.7$ cm^{-1}, $g = 1.98$, $|D(Mn^{III})| = 5.0$ cm^{-1} (fixed), $|D(Ni^{II})| = 10.0$ cm^{-1-1} (fixed), and TIP = 300×10^{-6} cm^3 mol^{-1}. It is to be noted that the evaluated exchange coupling between the terminal Mn(III) ions is parallel in nature and one

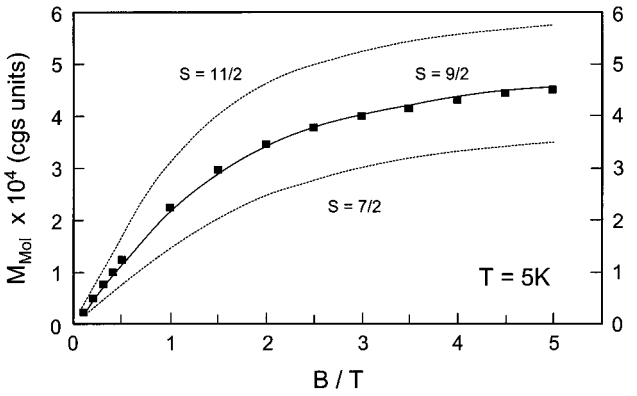

Figure 7. Plot of magnetization (■) versus the applied magnetic field for **5**. The solid line represents the Brillouin function for $S = {}^9/_2$ with $g = 1.97$. The dashed lines represent the theoretical magnetization curves for $S = {}^7/_2$ and $S = {}^{11}/_2$.

should not put too much weight on this value, although a small positive J_{13} was necessary to fit the experimental data. We addressed the point of global and local minima by consideration of the two-dimensional contour projection of the error surface. The error surface shows, in addition to a minimum with the above-mentioned "J" values, another minimum with the parameters $J \approx +23.9$ cm^{-1}, $J_{13} \approx -10.5$ cm^{-1}, and $g = 1.88$, which has been considered as a local minimum because of its large standard deviations. We conclude that the fitting procedure has correctly identified the global minimum and that uncertainties in the absolute magnitudes of J and J_{13} do not affect the conclusion that **2** has an $S_t = 3$ ground-state lying 32 cm^{-1} below the first excited state of $S_t = 2$.

The magnetic behavior of **6**, $Mn^{IV}Ni^{II}Mn^{IV}$, is quite characteristic of a ferromagnetic coupling. The solid line in Figure 5 shows the good quality of the fit with the following parameters: $J = +19.2$ cm^{-1}, $J_{13} = -10.1$ cm^{-1}, $g = 2.10$, $|D(Ni^{II})| = 10.0$ cm^{-1} (fixed). Although the quality of fit is nearly independent of $|D(Ni^{II})|$, we have kept it fixed to be consistent with the same for **2**. The evaluated lowest lying state of $S_t = 2$ lies only 2 cm^{-1} below the second lowest state of $S_t = 3$.

The magnetism of **3** can be interpreted in terms of an antiferromagnetic coupling between the neighboring high-spin Mn(III) ($S_{Mn} = 2$) and Cu(II) ion ($S_{Cu} = {}^1/_2$) and between the terminal Mn(III) ions, yielding an irregular spin-state structure with an $S_t = {}^7/_2$ ground state. The fit for **3** to the Heisenberg−Dirac−vanVleck (HDvV) model yielded antiferromagnetic coupling constants $J = -63.1$ cm^{-1} and $J_{13} = -2.8$ cm^{-1} with $g = 1.97$. To fit the low-temperature ($T < 15$ K) data, it was necessary to consider the $D(Mn^{III})$ parameter. The zero-field-splitting parameter $|D(Mn^{III})| = 5.0$ cm^{-1} was held constant during the fitting procedure. Local g_{Mn} dominates over local g_{Cu}, as can be seen in the molecular **g** tensor expressions[21,22] in determining the g values of complex **3**

$$g_{|7/2,4\rangle} = {}^{10}/_9 g_{Mn} - {}^1/_9 g_{Cu}$$

$$g_{|5/2,3\rangle} = {}^8/_7 g_{Mn} - {}^1/_7 g_{Cu}$$

which are in accord with the simulated g of less than 2.00. The first excited state with an $S_t = {}^5/_2$ lies at 40 cm^{-1} higher in energy than the ground state of $S_t = {}^7/_2$. A similar behavior

(21) (a) Chao, C. C. *J. Magn. Reson.* **1973**, *10*, 1. (b) Scaringe, R. P.; Hodgson, D. J.; Hatfield, W. E. *Mol. Phys.* **1978**, *35*, 701.
(22) Bencini, A.; Gatteschi, D. *EPR of Exchange Coupled Systems*; Springer-Verlag; Berlin, 1990.

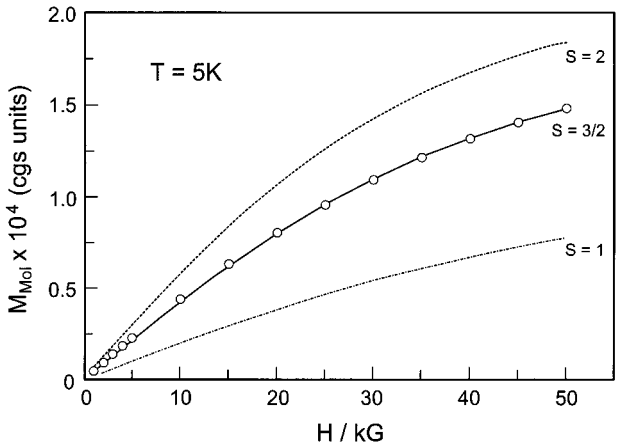

Figure 8. Field-dependent magnetization for **7**. The solid line is the simulation with the Brillouin function for $S = {}^3/_2$ with $g = 2.04$.

has been observed for the analogous $Fe^{III}Cu^{II}Fe^{III}$ compound,[6] for which the ground state was determined to have an $S_t = {}^9/_2$ with the first excited state having $S_t = {}^7/_2$. Contrary to the case of **3**, the coupling between Mn^{III} and Cu^{II} ions in the oxime-bridged compounds described in the literature[23] so far is ferromagnetic in nature.

An excellent fit of the magnetic data employing the HDvV model ($S_1 = S_3 = {}^3/_2$ and $S_2 = {}^1/_2$) for **7** yields $J = +72.7$ cm^{-1}, $J_{13} = -25.0$ cm^{-1}, and $g = 2.02$. It is interesting to note that the related isoelectronic $Cr^{III}Cu^{II}Cr^{III}$ complex[24] also exhibits ferromagnetism, but the exchange interaction is remarkably weaker ($J = +18.5$ cm^{-1}), which is attributable to the higher charge on the Mn(IV) center in **7** than that on the Cr(III) center. Completely parallel alignment of the spins leading to an $S_t = {}^7/_2$ is inhibited by the competing antiferromagnetic coupling between the terminal Mn(IV) centers in **7**. A strong influence of the long-range (~7 Å) exchange coupling on the spin ladder is responsible for the otherwise "excited state" of $S_t = {}^3/_2$ being the ground state for **7**. The g factors for the spin states $S_t = {}^3/_2$ and $S_t = {}^5/_2$, $g_{|3/2,1\rangle}$ and $g_{|5/2,2\rangle}$, respectively, are related to the local values $g_{Mn(IV)}$ and g_{Cu} by

$$g_{|3/2,1\rangle} = {}^3/_5 g_{Mn(IV)} + {}^2/_5 g_{Cu}$$

$$g_{|5/2,2\rangle} = {}^4/_5 g_{Mn(IV)} + {}^1/_5 g_{Cu}$$

indicating the dominance of $g_{Mn(IV)}$ over g_{Cu}, which is in complete accord with the evaluated g of 2.02.

Field-dependent magnetization at 5 K, shown in Figure 8, supports the energy ladder (Figure 9) evaluated from the susceptibility measurements. The solid line in Figure 8 is the simulation for the Brillouin function ($S = {}^3/_2$) with $g = 2.04$. The simulation of good quality shows that the ground state of $S_t = {}^3/_2$ is well separated ($\Delta E = 22.7$ cm^{-1}) from the excited state of $S_t = {}^5/_2$ and the zero-field splitting is negligibly small.

A preliminary report on the magnetic properties of **4** and **8** has been published.[10] Figures 4 and 5 display the new measurements down to 2 K for **4** and **8**. The theoretical value for two uncoupled spins of $S_1 = S_3 = 2$ with an average $g = 2.13$ is 7.38 μ_B, which is nearly identical with the measured

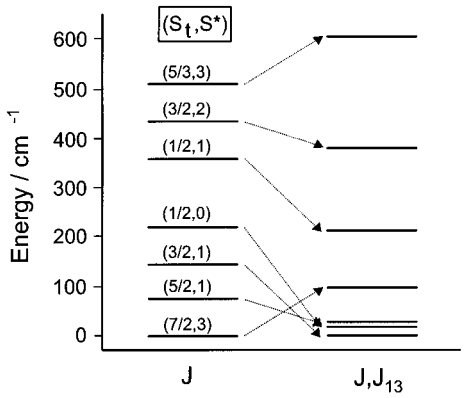

Figure 9. Spin-ladder for **7** with (right) and without (left) J_{13}.

magnetic moment value for **4** at 295 K. Accordingly, the best fit parameters with $S_1 = S_3 = 2.0$ and $S_2 = 0$ are $J_{13} = -0.4$ cm^{-1} and $g = 2.13$. The abrupt decrease in μ_{eff} below 20 K is presumably due to the sizable zero-field splitting of Mn(III).[25] **4** is X-band EPR-inactive at 4 K.

For **8**, a steady decrease of the magnetic moment with decreasing temperature is observed. This clearly indicates an $S_t = 0$ ground state for **8**, which is attained by a moderately strong antiferromagnetic coupling ($J_{13} = -19.2$ cm^{-1}) between two terminal Mn(IV) centers ($S_{Mn} = {}^3/_2$), separated by a large distance of ca. 7.0 Å. The low, but nonnegligible, magnetic moment has been attributed to 1.7% paramagnetic impurity of spin $S_{Mn}{}^{II} = {}^5/_2$. **8** is an example of the growing number of complexes that demonstrate the presence of intramolecular antiferromagnetic exchange coupling of considerable magnitude over distances >7 Å, provided the effective magnetic orbitals are favorably aligned.[2,26,27] EPR spectra of **8**, as expected, do not show any resonance below 30 K, corroborating the finding of antiferromagnetic coupling between two Mn(IV) centers in **8**.

We now provide a qualitative rationale for the trend and the nature of the exchange interactions between neighboring and between terminal spin carriers on the basis of the established Goodenough−Kanamori rules[28] for superexchange.

The evaluated exchange coupling constant can be factored into two opposing contributions from antiferromagnetic and ferromagnetic interactions

$$J = J_{AF} + J_F$$

with J_{AF} expressed as a negative term and J_F as a positive term.

Considering the O and N atoms of the bridging oxime groups as sp^2 hybridized, we will try to analyze the interaction parameters evaluated from the magnetic data. Hence, we will consider the different possible interactions[29] of the sp^2 orbitals on either side of the bridging oximate ligands with the different orbitals in idealized D_{3h} symmetry of the network Mn(O−N)$_3$M(N−O)$_3$Mn as a whole. The five metal d orbitals with

(23) (a) Birkelbach, F.; Winter, M.; Flörke, U.; Haupt, H.-J.; Butzlaff, C.; Lengen, M.; Bill, E.; Trautwein, A. X.; Wieghardt, K.; Chaudhuri, P. *Inorg. Chem.* **1994**, *33*, 3990. (b) Lloret, F.; Ruiz, R.; Julve, M.; Faus, J.; Journaux Y.; Castro, I.; Verdaguer, M. *Chem. Mater.* **1992**, *4*, 1150.
(24) Burdinski, D.; Birkelbach, F.; Weyhermüller, T.; Flörke, U.; Haupt, H.-J.; Lengen, M.; Trautwein, A. X.; Bill, E.; Wieghardt, K.; Chaudhuri, P. *Inorg. Chem.* **1998**, *37*, 1009.
(25) *Theory and Applications of Molecular Paramagnetism*; Boudreaux, E. A., Mulay, L. N., Eds.; Wiley: New York, 1976.
(26) Bürger, K. S.; Chaudhuri, P.; Wieghardt, K. *Chem.−Eur. J.* **1995**, *1*, 583.
(27) Gallert, S.; Weyhermüller, T.; Wieghardt, K.; Chaudhuri, P. *Inorg. Chim. Acta*, in press.
(28) (a) Goodenough, J. B. *Magnetism and the Chemical Bond*; Wiley: New York, 1963. (b) Goodenough, J. B. *J. Phys. Chem. Solids* **1958**, *6*, 287. (c) Kanamori, J. *J. Phys. Chem. Solids* **1959**, *10*, 87.
(29) (a) Kettle, S. F. A. *Symmetry and Structure*; Wiley: Chichester, U.K., 1985. (b) Krishnamurthy, R.; Schaap, W. B. *J. Chem. Educ.* **1969**, *46*, 799. (c) Allbright, T. A.; Burdett, J. K.; Whangbo, M.-H. *Orbital Interactions in Chemistry*; John Wiley & Sons: New York, 1985.

Scheme 1

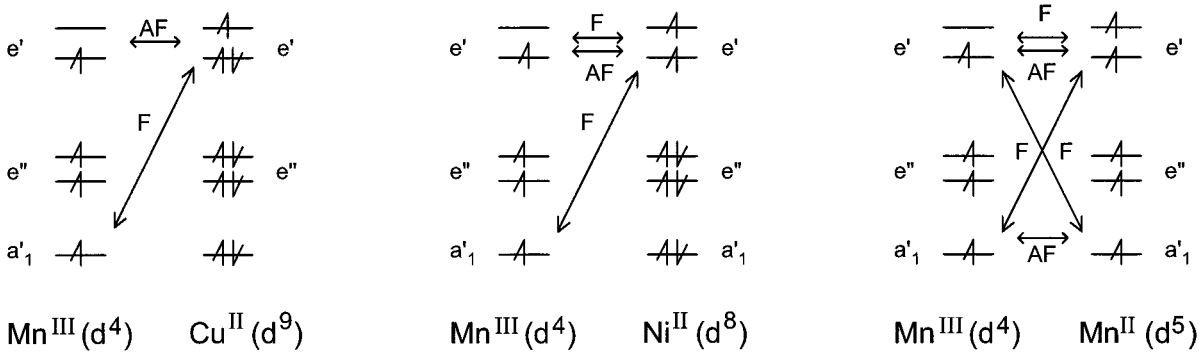

the 3-fold axis as the *z* axis along the Mn···M···Mn vector transform in D_{3h} symmetry as $a'_1(d_{z^2})$ $e''(d_{xz}, d_{yz}$: t_{2g} parentage), $e'(d_{x^2-y^2}, d_{xy}$: e_g parentage). The σ system (sp^2) is orthogonal to the a'_1 and e'' orbitals.

Scheme 1 shows the important exchange pathways operating in **1**−**3**. It is evident from the exchange coupling constant *J* of -63.1 cm^{-1} that the dominant exchange pathway for **3** is the symmetry-allowed $e'||sp^2||e'$ (using Ginsberg's symbols[30]) σ-superexchange pathway. Now, on going to the $Mn^{III}Ni^{II}Mn^{III}$ species, **2**, the strength of the overall antiferromagnetic interaction $-J$ decreases drastically from 63.1 to 5.3 cm^{-1}. The two unpaired electrons in the e′ orbitals of Ni(II) provide a ferromagnetic path, in addition to the antiferromagnetic path present in **3**, $Mn^{III}Cu^{II}Mn^{III}$, thus resulting in a reduction in the strength of the net antiferromagnetic spin coupling. The $J(e'|e')$ path still dominates the overall interaction. The central NiN_6 core in **2** is expected to be more twisted toward an octahedron than the corresponding core CuN_6 in **3**. In other words, the coordination polyhedron around Ni(II) in **2** deviates more from a trigonal prismatic arrangement as is found in $Mn^{III}Cu^{II}Mn^{III}$. This distortion from a trigonal prism decreases again the overlap between the magnetic orbitals of Mn(III) and Ni(II). Both of these effects together might cause the drastic reduction in the overall antiferromagnetic coupling for **2**. A similar reduction in the strength of the antiferromagnetic coupling has been observed in changing the central metal ion from Cu^{II} to Ni^{II} for the Fe(III)-system, i.e., the antiferromagnetic spin coupling in $Fe^{III}Cu^{II}Fe^{III}$ is stronger than that in $Fe^{III}Ni^{II}Fe^{III}$.[7]

Now we turn to the $d^4d^5d^4$ case in **1**. The ferromagnetic contributions provided by the $(a'_1,e'')\perp sp^2||(e')$ exchange paths now exceed those from the dominant $e'||sp^2||e'$ antiferromagnetic interaction, leading to an effective parallel spin coupling.

Let us now consider the $d^3d^9d^3$ (**7**), $d^3d^8d^3$ (**6**), and $d^3d^5d^3$ (**5**) cases. It is easy to envisage that removal of the electrons from the e′ orbitals leads to overall parallel spin coupling for all three compounds, **7**, **6**, and **5**, because the dominant antiferromagnetic AF paths present in **1**−**3** are missing for **5**−**7**. The ferromagnetic interaction in **5** is not stronger than that in **6** due to an additional antiferromagnetic path $a'_1||a'_1$.

Appreciable spin coupling is observed between the terminal metal ions ($J \approx -20$ cm^{-1}) separated by a large distance of ca. 7.0 Å. Unfortunately we could not obtain X-ray-quality crystals for **5**−**8**, but the structures of $Mn^{IV}Cu^{II}Mn^{IV}$ and $Mn^{IV}Zn^{II}Mn^{IV}$ with cyclohexanone dioxime[31] as the oxime ligand have been solved and the Mn(IV)···Mn(IV) distances have been found to be 7.064 and 6.974 Å, respectively. In this connection, we note that the higher covalent character of the Mn(IV)−ligand bond leads to stronger electronic interactions.

The π-conjugated system of the oxime ligand, delocalized over all bridging groups and perpendicular to the plane of the oxime ligand, appears to provide the dominant antiferromagnetic interaction between the terminal ions.

Concluding Remarks

The results described in the present paper show that it is possible to stabilize the tris(dimethylglyoximato)metalate(II) tetraanion by complexation with the LMn^{3+} or LMn^{4+} unit. (Glyoximato)metalate(II) anions are capable of functioning as bridging ligands to give rise to linear homo- and heterotrinuclear complexes and can mediate a varying range of exchange interactions, weak to moderate antiferromagnetic and even ferromagnetic. Because of their quasi-isostructural nature, these materials are unique and ideally suited for the study of intramolecular exchange interactions between three paramagnetic transition metal ions as a function of their respective d^n electron configurations.

This paper confirms the essentially σ nature of the interactions between the neighboring ions, and depending on the electronic configurations, these interactions may be antiferro- or ferromagnetic.

This study also confirms that there are indeed two different coupling constants, $J_{12} = J_{23} = J$ and J_{13}, operative in these linear trinuclear complexes; J_{13} is operative between two terminal paramagnetic centers separated by as large as ∼7 Å. The conjugated π-system of the bridging ligand appears to provide the dominant antiferromagnetic interaction between the terminal metal ions.

Complexes of the type $M_AM_BM_A$ exhibit irregular spin-level structures.[3] The level ordering is a result of the mutual influence of two different interactions which may lead to ground-state variability. The phenomenon of ground-state variability has been unambiguously demonstrated for linear trinuclear complexes of the type $M_AM_BM_A$.

Interestingly, the coupling between Mn^{III} and Cu^{II} ions in **3** is antiferromagnetic in nature in contrast to thar reported[23] for oxime-bridged corresponding heteronuclear complexes.

Acknowledgment. Financial support of this work from the Fonds der Chemischen Industrie is gratefully acknowledged.

Supporting Information Available: Tables of crystal data and intensity measurements, interatomic bond distances and angles, positional and thermal parameters, and hydrogen atom coordinates (8 pages). Ordering information is given on any current masthead page.

IC970362G

(30) Ginsberg, A. P. *Inorg. Chim. Acta Rev.* **1971**, *5*, 45.
(31) Birkelbach, F.; Weyhermüller, T.; Lengen, M.; Gerdan, M.; Trautwein, A. X.; Wieghardt, K.; Chaudhuri, P. *J. Chem. Soc., Dalton Trans.* **1997**, 4529.